


Please cite the Published Version

Brittain, R, Liskiewicz, T , Morina, A, Neville, A and Yang, L (2023) Diamond-like carbon graphene nanoplatelet nanocomposites for lubricated environments. Carbon, 205. pp. 485-498. ISSN 0008-6223

DOI: <https://doi.org/10.1016/j.carbon.2023.01.061>

Publisher: Elsevier

Version: Published Version

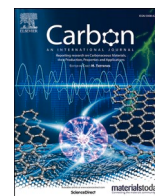
Downloaded from: <https://e-space.mmu.ac.uk/631703/>

Usage rights:  [Creative Commons: Attribution 4.0](#)

Additional Information: This is an Open Access article published in Carbon, by Elsevier.

Enquiries:

If you have questions about this document, contact openresearch@mmu.ac.uk. Please include the URL of the record in e-space. If you believe that your, or a third party's rights have been compromised through this document please see our Take Down policy (available from <https://www.mmu.ac.uk/library/using-the-library/policies-and-guidelines>)



Diamond-like carbon graphene nanoplatelet nanocomposites for lubricated environments

Rob Brittain^{a,*}, Tomasz Liskiewicz^b, Ardian Morina^a, Anne Neville^a, Liuquan Yang^{a,**}

^a Institute of Functional Surfaces, School of Mechanical Engineering, University of Leeds, LS2 9JT, UK

^b Faculty of Science and Engineering, Manchester Metropolitan University, M15 6BH, UK

ABSTRACT

The tribological behaviour of diamond-like carbon (DLC) and graphene nanoplatelets (GNP) nanocomposite has not been previously explored in a lubricated environment, with some previous studies reporting only on graphene materials on the surface of the DLC. In this study DLC-GNP nanocomposite films with various GNP coverages were synthesised by a 3 step process: spin coating a GNP suspension, heat treatment, and DLC deposition. In this study, the effect of the GNP coverage on the mechanical properties, and tribological response of the DLC-GNP nanocomposite film were studied at elevated temperatures against a cast iron pin in a base-oil lubricated environment. The study shows decrease in friction and wear of the DLC-GNP nanocomposites as the GNP coverage increased, with the lowest friction (COF ~ 0.03) and wear ($\sim 1.6 \times 10^{-19} \text{ m}^3/\text{Nm}^{-1}$) achieved with a 4.5% coverage. This study reports the addition of GNP into the DLC matrix reduced both friction and wear by creating a highly graphitic transfer film on the counter-body, but for higher GNP coverages agglomeration during the spin coating of GNP islands were recorded, leading to removal of the GNP during sliding wear negating the friction reduction effect of the GNP.

1. Introduction

Diamond-like carbon (DLC) is a well-known protective coating used due to the advantageous properties of low friction, low wear, high hardness and chemical inertness, making it suitable for use in a wide range of high pressure, or harsh environments [1–4]. The term DLC encompasses a wide variety of amorphous carbons, with classification dependent on their sp^2/sp^3 and hydrogen content [5]. The mechanical properties of DLC is related to the sp^2/sp^3 content, with the sp^3 (σ -bonds) fractions responsible for the high hardness, forming an amorphous network, with sp^2 (π -bond) graphitic clusters contributing to low friction [6]. The tribological performance of DLC has been reported to be environmentally dependent [7–9], with highly hydrogenated DLC coatings displaying superlubricity under high vacuum or nitrogen environments, but as humidity increases, the friction and wear increases dramatically, due to breakdown of the hydrogen at the interface increasing the adhesive covalent bonding between neighbouring dangling σ -bond. The elimination of adhesive σ -bonds interactions between articulating surfaces has shown to achieve ultra-low friction in tetrahedral amorphous carbon (Ta-C) where glycerol was found to saturate σ -bonds indicating these interactions are a significant contributor to friction [10,11]. Achieving superlubricity under demanding and realistic oil boundary lubricated conditions for amorphous

hydrogenated carbon (a-C:H) films has not been previously reported. For low friction in boundary lubricated a-C:H to be achieved the formation of a graphitic transfer-film on the counter-body is reported to be necessary [12]. The formation of a graphitic transfer film is achieved by an velocity accommodation model (VAM) where the transfer of material from the DLC film onto the counter-body during sliding contact, where a structural in change by mechanical shear strain at the interface induces sp^3 carbons into a lower energy sp^2 graphitic configuration [13–15]. This graphitic transfer layer on the counter-body creates a low shear sliding interface, although other mechanisms focusing on a-C passivation show promise to explaining the low friction and wear in a DLC system [16,17].

Graphene is a relatively new material, and has garnered scientific and engineering interest due to the exceptional in-plane mechanical strength, that theoretically makes it a high-performing ultra-thin protective coating [18,19]. Graphene differentiates itself from DLC by containing only sp^2 -hybridised carbons atoms which are arranged in an atomically flat 2-dimensional (2D) single layer honeycomb structure [20]. The 2D arrangement of the carbon atoms makes single layer graphene (SLG) a suitable candidate for displaying superlubricity by incommensurate sliding [21,22]. However, the frictional response of graphene is affected by a number of factors namely: substrate adhesion, defects, environment, and the number of layers, compounded by the

* Corresponding author.

** Corresponding author.

E-mail addresses: py06rb@leeds.ac.uk (R. Brittain), L.Q.Yang@leeds.ac.uk (L. Yang).

<https://doi.org/10.1016/j.carbon.2023.01.061>

Received 3 August 2022; Received in revised form 30 January 2023; Accepted 31 January 2023

Available online 31 January 2023

0008-6223/© 2023 The Authors. Published by Elsevier Ltd. This is an open access article under the CC BY license (<http://creativecommons.org/licenses/by/4.0/>).

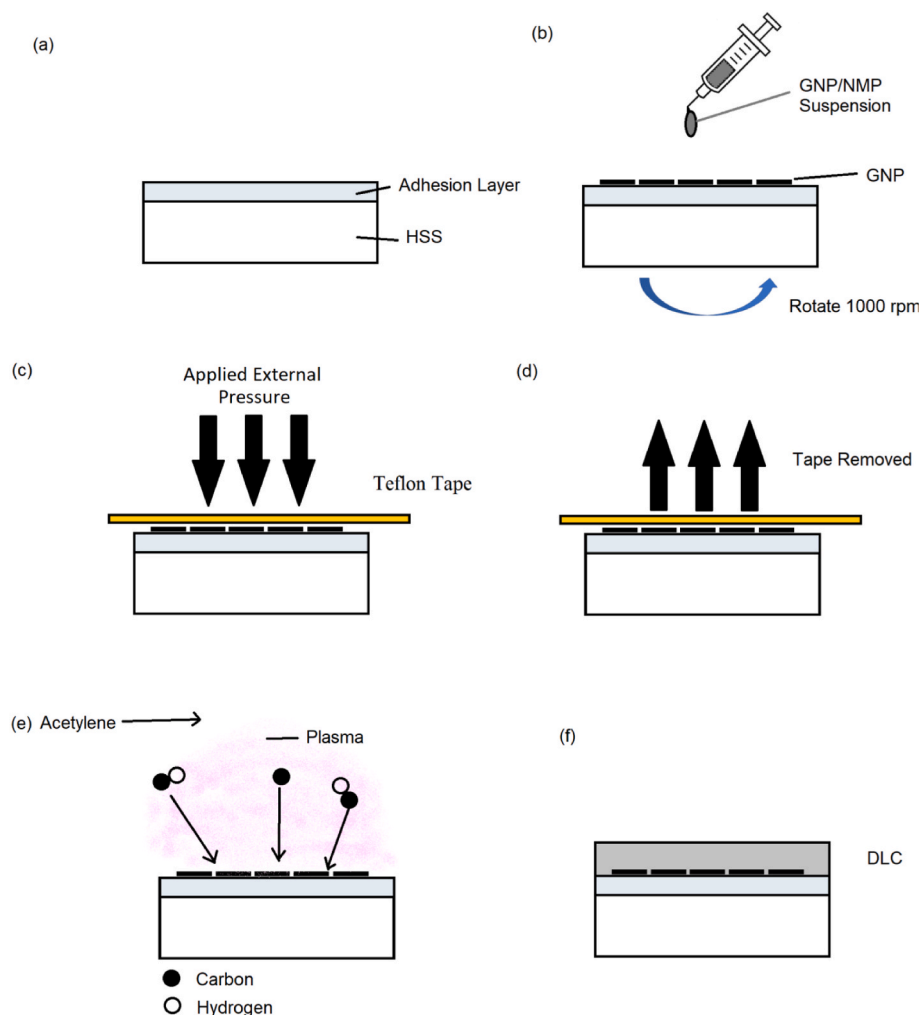


Fig. 1. Schematic flow diagram for DLC-GNP synthesis. (a) HSS steel coupon with interlayer, (b) drop cast spin coating GNP-NMP suspension, (c) Teflon tape pressed onto GNP coated surface, and heated at 200°C for 3 h, (d) tape removal and cleaning, (e) DLC deposition, and (f) resulting DLC-GNP composite structure. (A colour version of this figure can be viewed online.)

difficulties in transferring or growing graphene on to a substrate [23–26]. The difficulties in the effective application of graphene, has shown graphene nanoplatelets to be a useful alternative; maintaining many of the attractive properties of graphene while being easier to handle, and cheaper to synthesise [27]. PEEK or PMMA nanocomposites containing GNP are shown to be effective at reducing both friction and wear by creating a thin graphitic low shear strength transfer layer between the counter-body and the nanocomposite [28–30]. However, Ervin et al. [31] observed clustering of GNP within a composite, which can act as defect points, propagating cracks through the composite. The formation of a transfer layer is reported by Bhowmick et al. [32] where MLG (multi-layer graphene) sliding against DLC formed a graphene transfer layers on the counter-body. The low friction achieved was due to passivating the two articulating surfaces, the DLC by hydrogen (H) atoms and graphene by H and OH. Another friction reduction mechanism of graphene is by the formation of graphene nanoscrolls on the surface of DLC, reducing the real area of contact with superlubricity recorded [33,34]. Although the mechanism relies on very controlled environments which may not be suitable for a wide variety of real world engineering applications [33,34].

The synthesis of DLC embedded with graphitic nanomaterials (carbon nanotubes or graphitic-like carbons) is a relatively recent and promising proposal, displaying enhanced tribological performance [35–37]. The critical friction reduction mechanisms of these graphitic nanocomposites is reportedly through increased graphitization lowering

the adhesive shear, or stress distribution lowering the real area of contact. This study considers a different approach that currently employed in a cam follower environment to reduce both friction and wear. Typically in these type of lubricated contacts, the use of environmentally damaging additives, or reduction in viscosity is used to either protect the surface or increase the efficiency [38–41].

In this study we report the synthesis of DLC-GNP nanocomposites with various coverages of GNP. These nanocomposites are synthesised by combining a drop cast spin-coating various concentrations of GNP suspension, heat treatment and DLC deposition. The effect of GNP concentration on the mechanical properties, along with the lubricated tribological response under elevated temperature are discussed along with the surface morphology. Raman spectra analysis is used to characterize the graphitization of the films and counter-body after wear, along with scanning electron microscopy, and transmission electron and EELS spectroscopy. A mechanism is proposed for the low friction and wear that have been observed.

2. Methodology

2.1. Diamond-like carbon– graphene nanoplatelet nanocomposite synthesis

The synthesis of the DLC-GNP composite films is shown in Fig. 1 and completed on polished high speed steel (HSS) coupons (6 mm thickness,

Table 1

DLC deposition conditions in the Hauzer Flexicoat 850 system by PECVD.

Process	Time (minutes)	Argon gas flow (sccm)	C ₂ H ₂ gas flow (sccm)	Bias DC (V)	UBM coil current (A)
Pumping	60	–	–	–	–
Plasma etch	20	50	–	–200	–
a-C:H deposition	90	–	340	–740	4

Table 2

Tribological test conditions.

Test Conditions	Value
Entrainment speed	20 mm/s
Load	280 N
Temperature	100 °C
Lubricant	Poly- α -olefin (PAO) $\eta_0=3.1$ mPaS at 100 °C
Counter material	Cast Iron 40 mm equivalent radius
Test duration	6 h

Table 3

Material properties used in tribological tests.

	Substrate	Counter material
Material	M2 HSS Steel	Cast Iron
Roughness (R_a)	18 ± 4 nm	73 ± 26 nm
Young's Modulus	210 GPa	170 GPa
Dimensions	15 mm diameter 6 mm thickness	20 mm length 6 mm diameter 40 mm curvature radius

30 mm diameter) coated with an Cr/WC/W layer previously used to aid DLC adhesion [42]. The GNP were suspended in N-Methyl-2-pyrrolidone (NMP) by ultra-sonication for 6 h at concentrations between 0.25 and 2 mg/ml. The GNP were purchased commercially from Sigma Aldrich having a typical surface area of 120–150 m²/g, average thickness of 6–8 nm and particle size of 5 μ m. The GNP were deposited onto the surface of the adhesion layer by drop cast spin coating using 1 ml of the GNP/NMP suspension at 1000 rpm for 1 min and left to dry.

A heat treatment process was used to improve adhesion of GNP to the substrate. Heat treatment consisted of Teflon tape pressed tightly onto the GNP coated adhesion layer, and then placed in an oven at 200 °C for 3 h. The tape was removed, cleaned in an ultrasonic bath of acetone for 5 min, followed by 5 min in ethanol to remove any NMP residue. The DLC layer was deposited on top of the GNP coated coupon by plasma enhanced chemical vapour deposition (PECVD) using an industrial size Hauzer Flexicoat 850 system with acetylene used as the precursor gas. The DLC deposition conditions are shown in Table 1.

In total 5 GNP/NMP concentrations were used during spin coating process; 0, 0.25, 0.5, 1 and 2 mg/ml. These fully synthesised nanocomposites are denominated by DLC-GNPX, where “X” refers to the GNP/NMP concentration used. A pure (0 mg/ml) DLC sample was used as a baseline comparison, created simultaneously but without GNP.

2.2. Tribological testing

The tribological tests were conducted at University of Leeds using a Biceri pin-on-flat reciprocating tribometer with a cast iron (CI) counterbody. The test conditions and material properties are given in Table 2 and Table 3 accordingly. A poly- α -olefin (PAO) Group (IV) base oil was chosen to ensure that no interactions from additive packages would be present. The elevated temperature (100 °C) was used to simulate that experienced in a demanding high load environment such as a cam follower in the internal combustion engine. The initial contact pressures were calculated for each sample using the Hertzian contact pressure equations [43].

To determine the lubrication regime, the load, material and lubricant

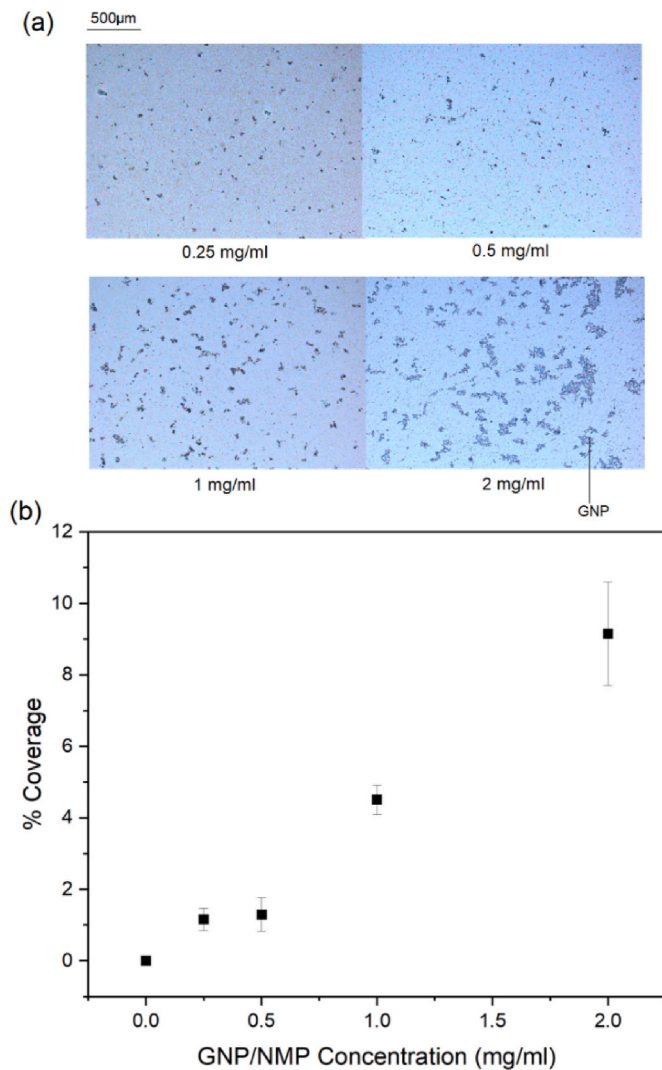


Fig. 2. (a) Optical image of DLC-GNP films synthesised from various GNP/NMP concentrations and (b) the percentage of GNP coverage as a function of the GNP/NMP concentration used. (A colour version of this figure can be viewed online.)

properties were used in Equations 1 and 2 [44]. To calculate a numerical value for the minimum film thickness:

$$\frac{h_{min}}{R'} = 3.63 \left(\frac{U\eta_0}{E'R'} \right)^{0.68} (\alpha E')^{0.49} \left(\frac{W}{E'R'^2} \right)^{-0.073} (1 - e^{-0.68k}) \quad (\text{Equation 1})$$

Where R' is the reduced radius of the two surfaces in contact, α is the viscosity–pressure coefficient (1.1×10^{-8} Pa^{−1}), η_0 is the dynamic viscosity, U is the entraining surface velocity of the pin, W is the load and E' is the reduced elastic modulus. The lambda ratio (λ) is calculated using:

$$\lambda = \frac{h_{min}}{\sqrt{R_{a1}^2 + R_{a2}^2}} \quad (\text{Equation 2})$$

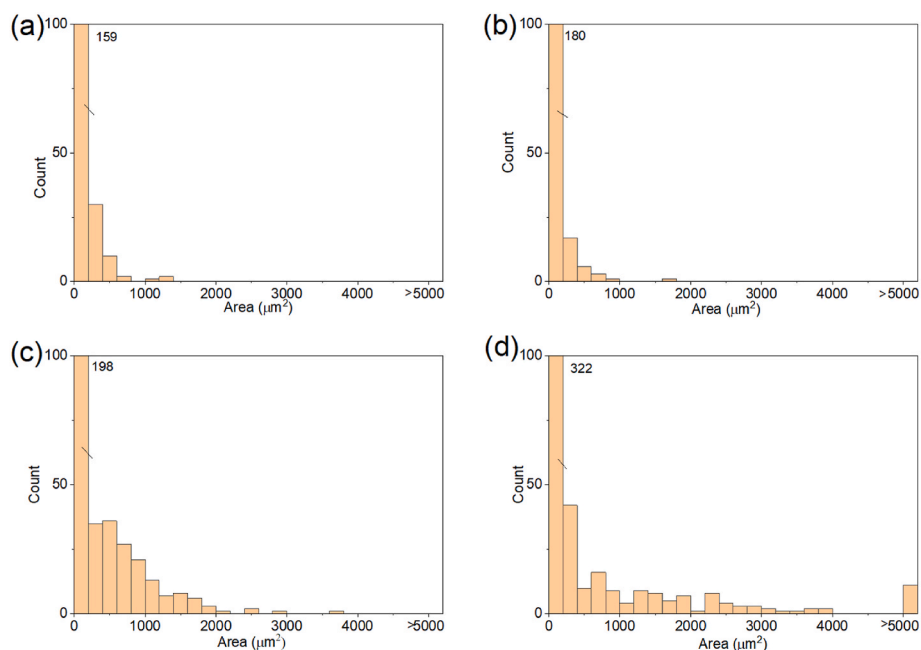


Fig. 3. GNP island size distribution for (a) 0.25 mg/ml, (b) 0.5 mg/ml, (c) 1 mg/ml and (d) 2 mg/ml GNP/NMP concentration. (A colour version of this figure can be viewed online.)

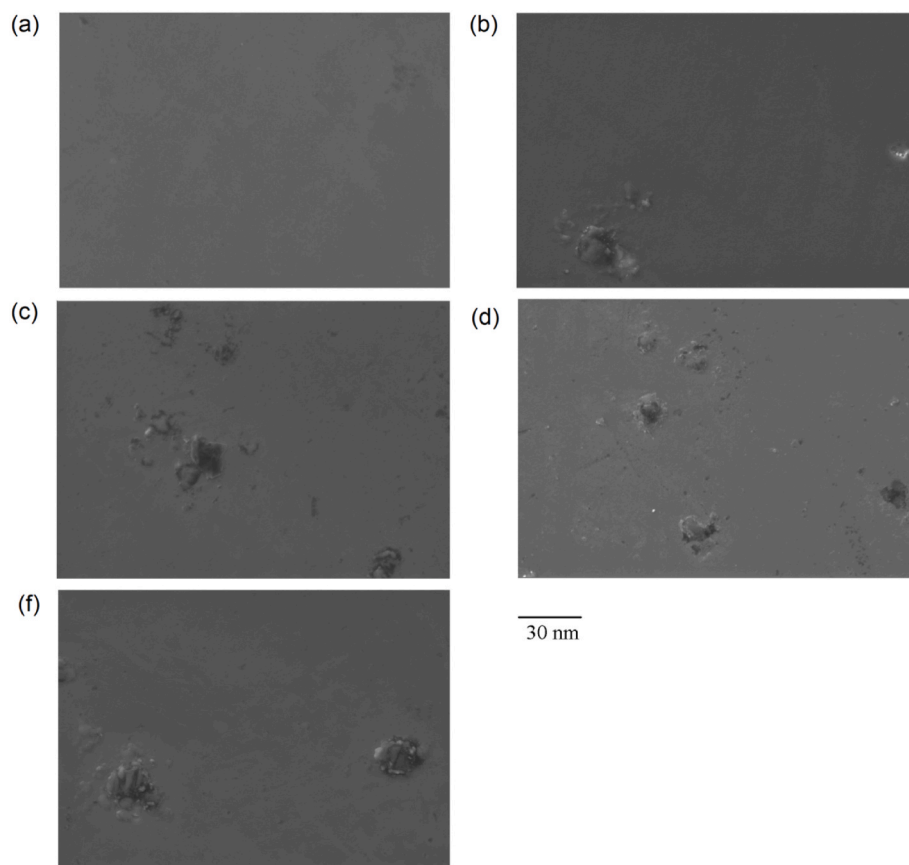


Fig. 4. SEM topography of as-deposited (a) pure DLC, (b) DLC-GNP0.25, (c) DLC-GNP0.5, (d) DLC-GNP1 and (e) DLC-GNP2 films. (A colour version of this figure can be viewed online.)

Where R_{a1} and R_{a2} are the mean surface roughness of the film, and CI pin respectively. The calculated λ value for all DLC-GNP nanocomposites tested are in the range 0.028–0.049 signifying that it is predicted to be in

the boundary regime.

Surface roughness measurements were taken using a Bruker NPFlex 3D optical profiler using white light interferometry (WLI) with a vertical

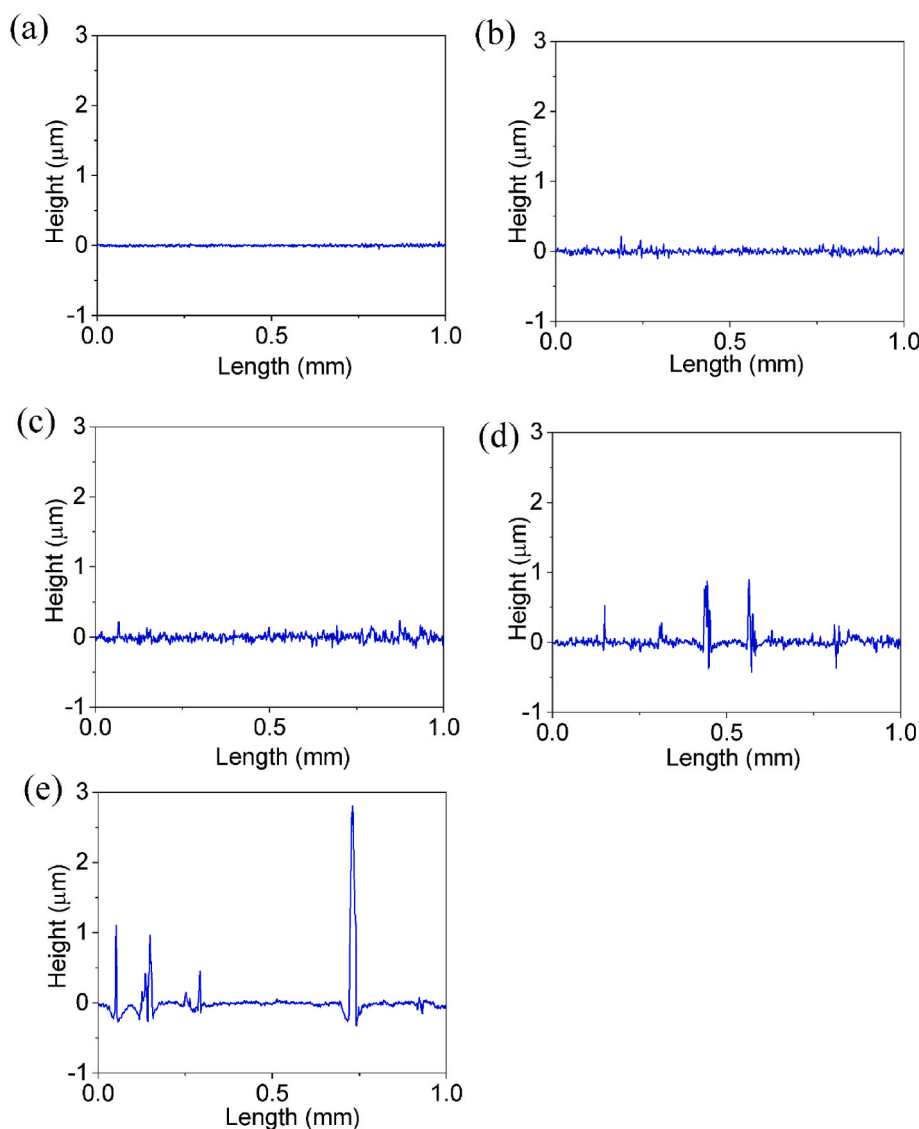


Fig. 5. Representative line scans taken of as-deposited (a) pure DLC, (b) DLC-GNP0.25, (c) DLC-GNP0.5, (d) DLC-GNP1 and (e) DLC-GNP2 films. (A colour version of this figure can be viewed online.)

Table 4

Mean surface roughness (R_a) for DLC-GNP samples.

Sample	R_a (nm)
Pure DLC	21 ± 1
DLC-GNP0.25	33 ± 13
DLC-GNP0.5	49 ± 2
DLC-GNP1	77 ± 6
DLC-GNP2	112 ± 49

resolution of <0.15 nm measuring surface roughness profiles, and analysed using the Vision64 software package. Surface roughness measurements were taken from 5 random spots on each sample, with the software calculating the mean surface roughness (R_a). The wear volume for the DLC-GNP films was measured by WLI in 3 different areas of the wear track after each test ($n = 3$), with the average value of the cross-sectional volume measured and the wear coefficient calculated using the Archard wear equation [45]. The wear rates of the pins were calculated by optical microscope measuring the wear scar diameter, which was used to calculate the removed volume of the sphere. Once the missing volume was calculated, the Archard wear equation was used to

determine the specific wear rate [46].

2.3. Characterisation

The GNP distribution was characterised using a Lecia 800 M optical microscope, with surface coverage of GNP measured using ImageJ software. Five random areas were measured with the mean and standard deviation calculated. Scanning electron microscope (SEM) micrographs of the surface before and after tribological tests were taken using the Carl Zeiss EVO MA15 SEM. Cross-sections of as-deposited DLC-GNP nanocomposites were prepared using a FEI Helios G4 CX DualBeam SEM with Focused Ion Beam. The TEM images and electron energy loss spectroscopy (EELS) spectra were obtained using the FEI Titan3 Themis 300: X-FEG 300 kV S/TEM. The accelerating voltage was set to 300 kV, and the EELS spectra undertaken using magic angle conditions eliminating any orientation dependent contributions commonly experienced with 2D materials [47]. The full width half maximum (FWHM) of the zero loss peak was 1 eV and dispersion was 0.1 eV/pixel. The C K-edge was collected for 30s and the low loss was collected for 0.002s. The EELS spectra was analysed to characterize the sp^2 bonded carbon content using Gatan's Digital Micrograph software by the method proposed by

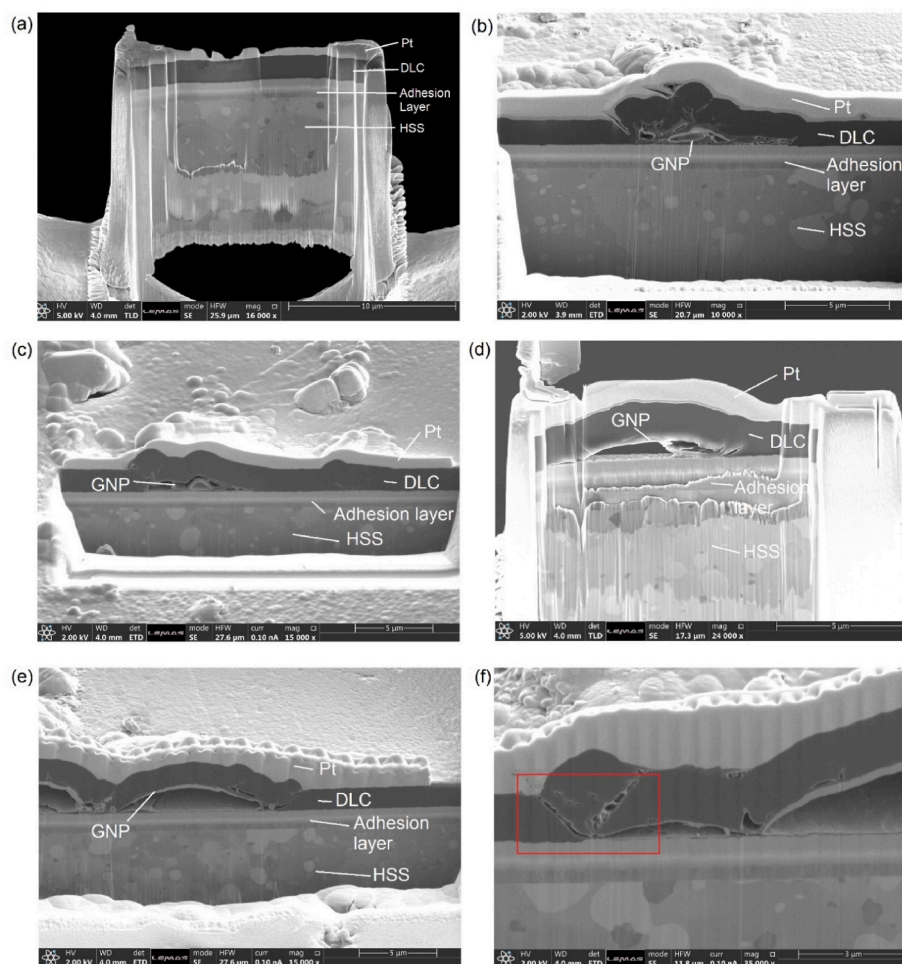


Fig. 6. Cross sections of (a) pure DLC, (b) DLC-GNP1 (type 1 structure), (c) DLC-GNP1 (type 1 structure), (d) DLC-GNP1 (type 2 structure), (e) DLC-GNP2 and (f) DLC-GNP2 nanocomposites with the red box indicating an area with a void through to the surface. (A colour version of this figure can be viewed online.)

Zhang et al. [48]. The spectra for the DLC-GNP was taken at the adhesion layer/GNP interface, GNP/DLC interface, and at varying thickness of the DLC layer.

Mechanical properties were obtained using a Micro Materials Nano Vantage using depth controlled indentation at a 10% maximum coating thickness (100 nm). A loading and unloading rate of 0.2 mN s^{-1} along with an initial contact load of 0.01 mN was applied. A 60 s dwell period was observed post-indentation to account for thermal drift. A total of 100 indentations were performed per coating for the bulk mechanical properties with a separation distance of $25 \mu\text{m}$. Single targeted indentations were completed with 10 indents for each feature (the GNP islands, and DLC areas) for all samples.

Raman spectroscopy is a non-destructive characterisation technique commonly used for both GNPs and DLC to measure both damage to GNPs, and graphitization of DLC after wear [49,50]. Raman spectra were collected using a Renishaw inVia (UK) Raman spectrometer at a wavelength of 488 nm, spot size of 400 nm, and collected within the ranges of $900\text{--}2000 \text{ cm}^{-1}$. Measurements were taken on both the pin and DLC-GNP before and after tribological tests. To preserve any graphitic transfer film after testing, sample surfaces and pins were gently rinsed in heptane to remove the PAO base-oil. The DLC-GNP has discrete islands of GNP, so spectra were taken from both the 'GNP islands' and 'DLC area'. The spectra were analysed using OriginPro 2017 Edition with the D and G peak deconvoluted into their respective Gaussian peaks, which has shown to produce accurate results [51]. The I_D/I_G ratio was taken from the deconvoluted peaks, and used to determine the graphitization after wear [52,53]. Data from 10 random spots before wear were taken,

along with spectra from the centre of the wear scar, and CI pin with the average values and standard deviation calculated.

3. Results and discussion

3.1. GNP distribution and surface morphology

Fig. 2 shows the coverage percentage as a function of GNP/NMP concentration, with the minimum GNP coverage of $\sim 1.16\%$ and $\sim 9.15\%$ being the highest. The GNP form small discrete islands at the lower concentrations, however begin to agglomerate as the concentration used increases.

The GNP island size distribution is shown in Fig. 3. The area of the GNP islands increases, with increasing concentration. The 0.25 mg/ml GNP/NMP suspension produces relatively small islands with $0\text{--}200 \mu\text{m}^2$ the most dominant range. The 0.5 mg/ml increases the amount of islands in the $0\text{--}200 \mu\text{m}^2$ range. The 1 mg/ml suspension produced similar results in the $0\text{--}200 \mu\text{m}^2$ range, but larger island areas emerging up to $2000 \mu\text{m}^2$. The highest concentration (2 mg/ml) GNP/NMP suspension produced more small islands, but also much larger islands above $5000 \mu\text{m}^2$.

SEM along with WLI (Fig. 4 & Fig. 5) was used to observed the changes to the as-deposited DLC-GNP surface as the GNP/NMP concentration increased. The GNP islands were visible at the surface with line scans from WLI confirming the height increases with the higher concentration. The mean surface roughness (R_a) of the DLC-GNP was taken to allow an overview of the average roughness as the GNP/NMP

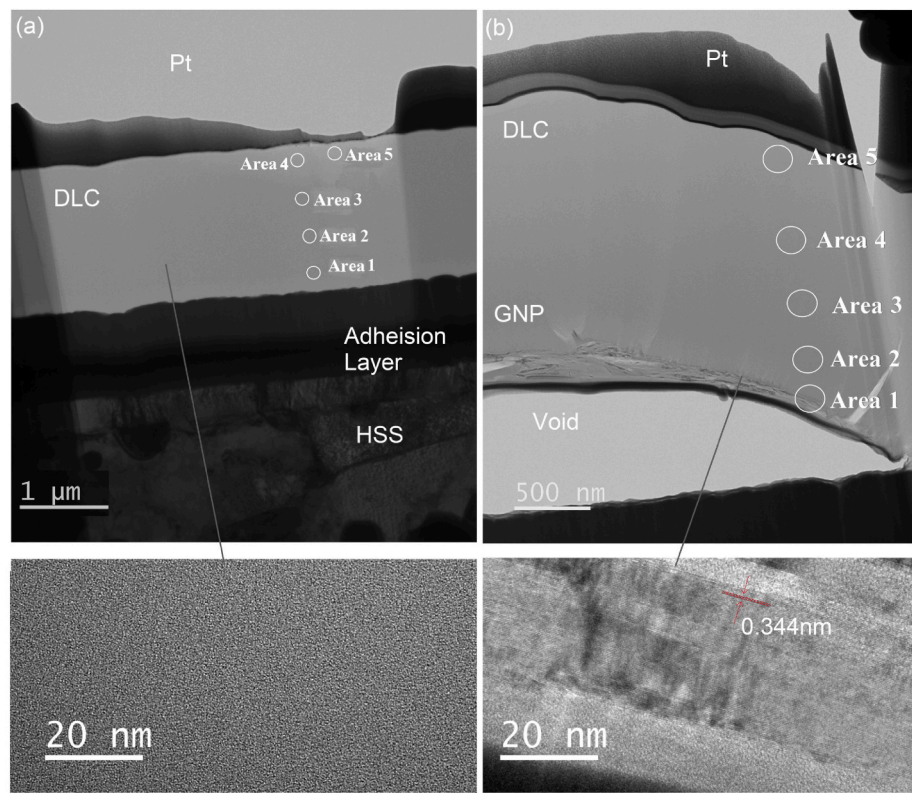


Fig. 7. Cross sections of (a) pure DLC and (b) DLC-GNP1, with the corresponding EELS scan areas, and HRTEM images of the corresponding linked areas. (A colour version of this figure can be viewed online.)

Table 5
 sp^2/sp^3 ratio for pure DLC and DLC-GNP1 at different sample depths.

Area	DLC $sp^2/sp^3\%$	DLC-GNP $sp^2/sp^3\%$
1	62.7	74.7
2	54.2	72.2
3	56.2	65.4
4	56.8	56.4
5	55.2	56.4

concentration is increased (Table 4). The DLC-GNP2 sample provides high peaks which are assumed to be the result of agglomeration presented previously in Fig. 3. These high peaks (increased surface roughness) have shown in other works to increase wear through greater asperity contact [54].

The R_a increases rapidly as the GNP/NMP concentration increases, which would correlate to the agglomeration seen in Fig. 2 for the higher concentrations. The increased R_a would result in more contact at these asperity points, increasing both friction and wear [54]. The maximum

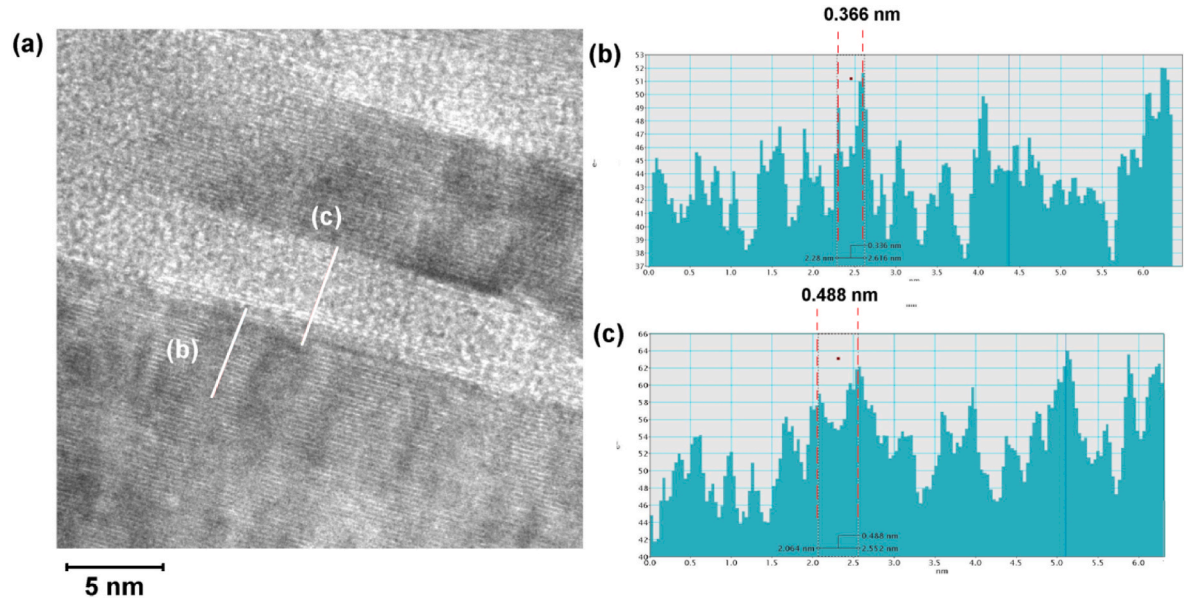


Fig. 8. (a) TEM micrograph with line scans of (b) GNP layer, and (c) amorphous layer. (A colour version of this figure can be viewed online.)

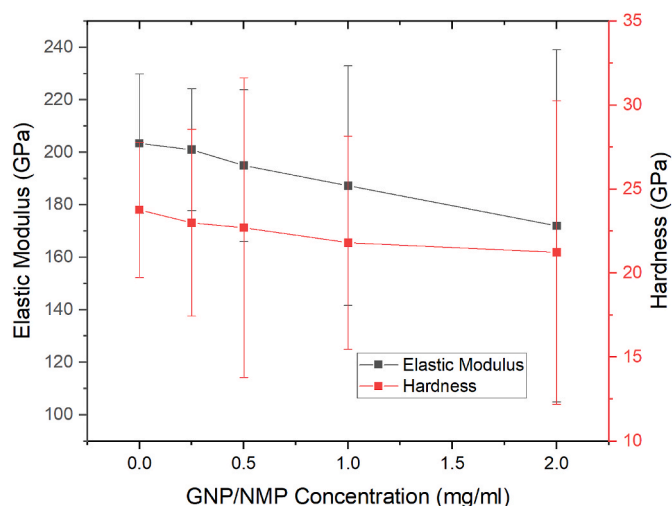


Fig. 9. Mechanical properties of DLC-GNP films as a function of GNP/NMP concentration. (A colour version of this figure can be viewed online.)

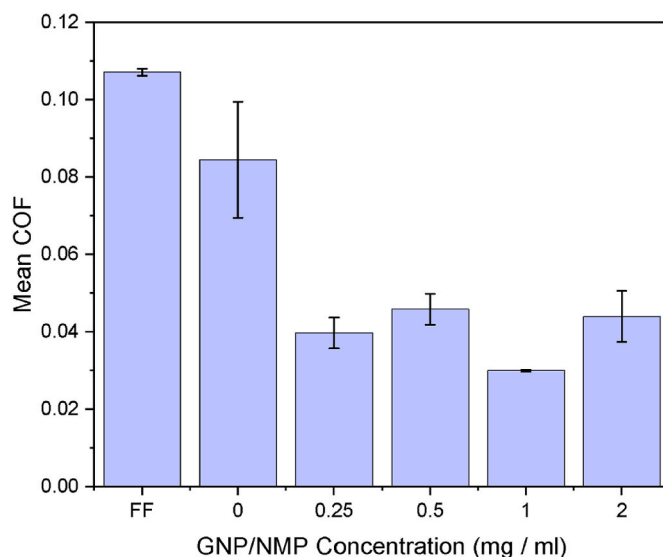


Fig. 11. Mean COF for steady state friction (last 3 h, $n = 3$). (A colour version of this figure can be viewed online.)

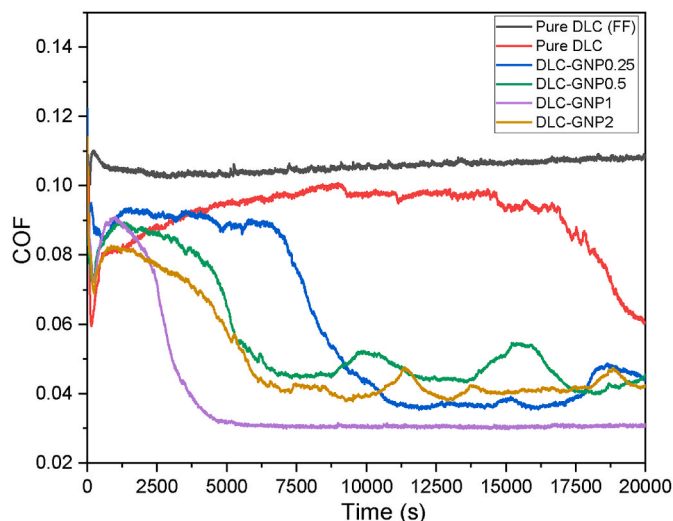


Fig. 10. Friction results for DLC-GNP composites for 6 h tests against a CI counter-body. (A colour version of this figure can be viewed online.)

Table 6

Initial contact pressure used for tribological test.

Sample	Initial contact pressure (MPa)
Pure DLC	715
DLC-GNP0.25	700
DLC-GNP0.5	694
DLC-GNP1	685
DLC-GNP2	666

peak height from the line scans, show very high peaks for the DLC-GNP1 and DLC-GNP2, which can be explained by the observation of Fig. 5 where some of the GNP islands are visible sticking through the coating to the surface.

Cross-sections of pure DLC, DLC-GNP1 and DLC-GNP2 are shown in Fig. 6. The addition of GNP into the DLC matrix introduces voids into the structure, which are visible in the cross-sections. The DLC-GNP1 structure presented two different GNP orientations; type 1 where the GNP is throughout the DLC structure with GNP edges penetrating through to the surface, and type 2 where the GNP is aligned parallel with the substrate, with no indication that the GNP is present near the top layer of

the DLC. The DLC-GNP2 structure presents larger voids than those observed in DLC-GNP1, with more GNP stacking. These large voids could act as sites of crack propagation, as was noted by Choleridis et al. for blistered DLC where similar topographical structures are observed [55].

Fig. 7 presents TEM cross-sections of pure DLC and DLC-GNP1. The pure DLC structure consists of an amorphous layer, while the DLC-GNP1 displays the amorphous DLC with a lamella structure present with a spacing of 0.344 nm, consistent with graphite [56]. The EELS spectra are taken from the areas indicated and the results calculated in Table 5. The pure DLC sp^2/sp^3 ratio has a deviation near the substrate/adhesion layer, but remains within 1%, for the remaining spectra moving towards the surface. The DLC-GNP1 has a high sp^2/sp^3 at the GNP area 1, indicating it is highly graphitic. The presence of an amorphous structure (sp^3 bonding) was also present within the EELS spectra taken at the GNP later, with 100% sp^2 content not observed. TEM micrographs presented in Fig. 8, with accompanying line scans show a ~ 0.366 nm reciprocity, where as the amorphous structure was larger at ~ 0.488 nm. The DLC-GNP1 displays more graphitic content up until area 4 where it reaches parity to the pure DLC sample. These results tie into the molecular simulation work completed by Liu et al. [57] where DLC is grown on MLG. The edge sites and surface of the GNP will have more energetically favourable sp^2 bonding sites, where some of the graphene layers are consumed during the deposition process due to ion implantation during film growth [57]. The outer most layers of the Pure DLC and DLC-GNP (Areas 4 & 5) are the layers that will initially be in contact with the CI counter. However when observing Fig. 6 (b) & (c) the GNP is closer to the surface and these would contribute to tribosystems during frictional tests.

3.2. Bulk mechanical properties

The bulk mechanical properties of the DLC-GNP films are shown in Fig. 9. The hardness and elastic modulus were affected by the GNP/NMP concentration used, where it decreases as the GNP/NMP concentration increases. However, the deviation is very high for all samples which would allow some overlap. These results support similar work completed by Kinoshita [36], where increases in CNT concentration reduced both hardness and elastic modulus, but differs from the results obtained by Dai et al. [58] and Wei et al. [35] where an increase was observed. The orientation of the carbon allotropes deposited could play an important factor with out of plane GNP ($E = 0.3\text{--}45.4$ GPa [59])

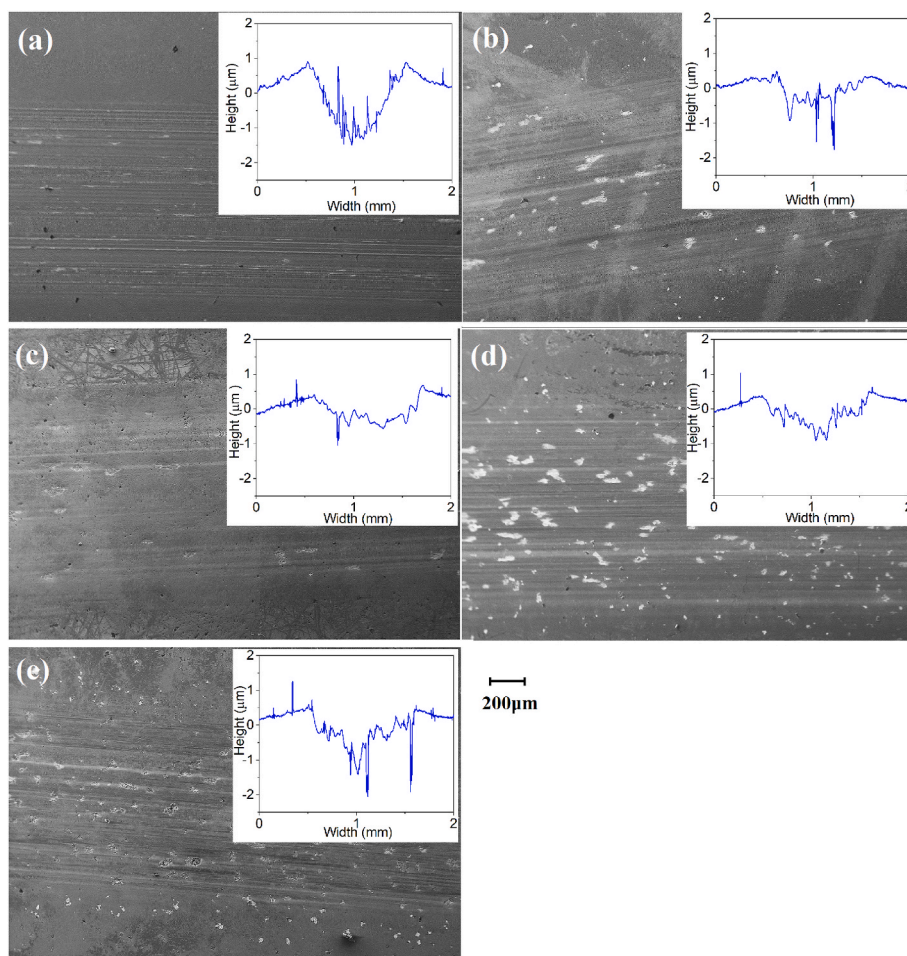


Fig. 12. SEM wear scar and representative line scan of (a) pure DLC, (b) DLC-GNP0.25, (c) DLC-GNP0.5, (d) DLC-GNP1 and (e) DLC-GNP2 films with the representative line scan wear scars. (A colour version of this figure can be viewed online.)

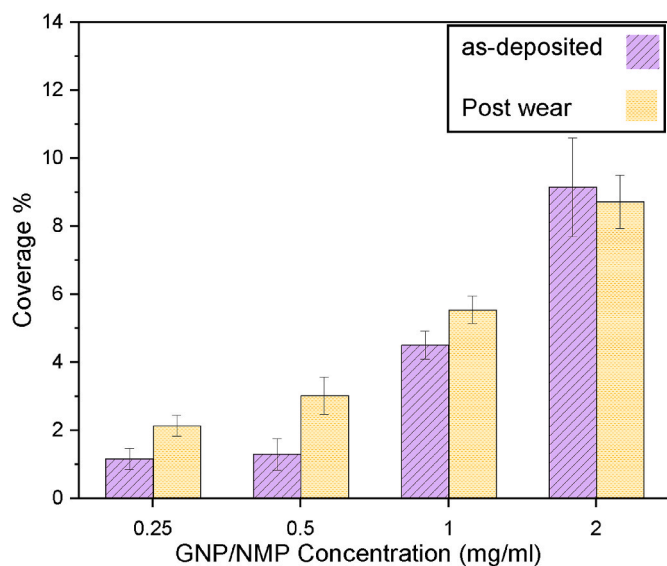


Fig. 13. GNP coverage for as-deposited DLC-GNP and post wear. (A colour version of this figure can be viewed online.)

considered to be a softer material than DLC ($E = 203$ GPa) so as the GNP coverage increases the bulk elastic modulus and hardness would decrease accordingly [60].

The high standard deviation observed could be the result of the indenter hitting GNP islands creating large differences in elastic modulus and hardness of the films. To test this theory such single point indentations were completed on each sample at the GNP islands ($n = 10$ for each sample). The results for indentations on the GNP islands presented results at much lower hardness and elastic modulus. It is quite evident that by taking into account Fig. 6, the voids around the GNP will yield under an applied load, leading to low elastic modulus at these points.

3.3. Tribological testing

The coefficient of friction (COF) as a function of sliding time is given in Fig. 10. The initial contact pressures using the bulk elastic modulus, along with the results from targeted point indentations at the DLC area and GNP islands are presented in Table 6. For the targeted indentations it is assumed that the contact area is 100% between the CI counter-body and discrete areas probed. When comparing the bulk contact pressures there is a decrease as the GNP/NMP concentration increases.

Contact pressure is important in DLC contact mechanics as it affects transfer film formation, and wear during tribological tests, with higher pressure reporting lower friction for a-C:H films [61,62]. The high variation in elastic modulus from the GNP islands within DLC matrix suggest there will be localised contact pressure differences during sliding, where the DLC matrix would produce higher areas of contact pressure increasing the graphitization at these points. Higher contact pressures increase the flash temperatures facilitating the phase

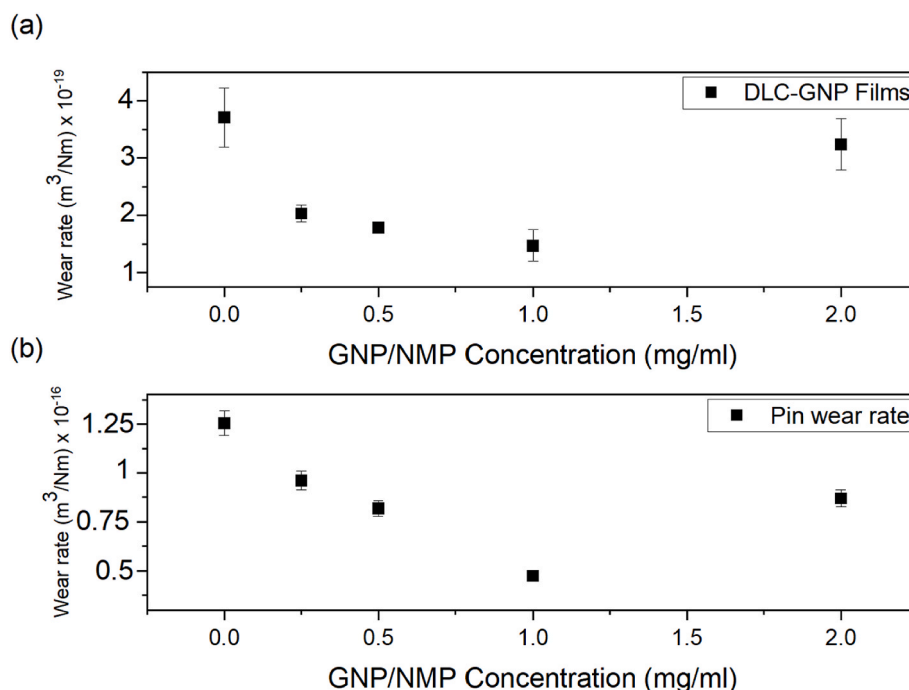


Fig. 14. Specific wear rate for (a) DLC-GNP nanocomposites and (b) CI pins. (A colour version of this figure can be viewed online.)

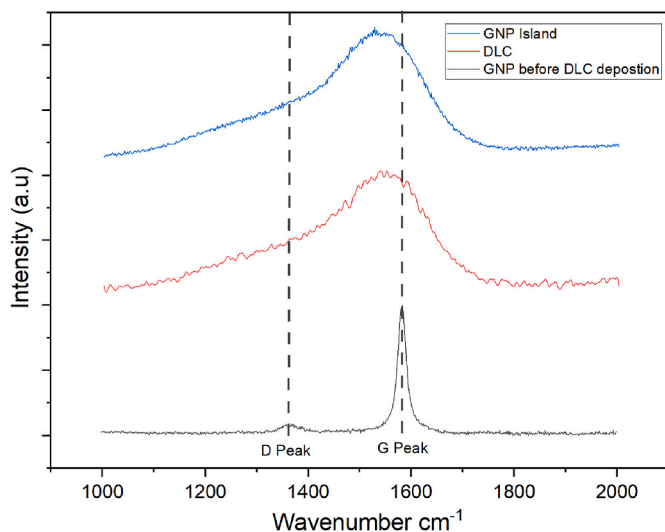


Fig. 15. Raman spectra of GNP before DLC deposition, along with DLC areas and GNP islands of DLC-GNP coating. (A colour version of this figure can be viewed online.)

transformation from sp^3 to sp^2 carbon bonding, which could be a mechanism for the lower friction as the GNP coverage increases [63,64].

The frictional response from the DLC-GNP nanocomposites display the typical DLC ‘wearing in’ behaviour; a sudden short lived decrease, followed by a sharp increase at the start of testing [65]. The pure DLC film sustains a high COF (~ 0.09) until 17,500 s where a reduction is observed. The introduction of GNP into the DLC matrix improves the frictional response for all DLC-GNP composites, compared to the pure DLC. The DLC-GNP0.25 friction taken the longest ($\sim 7,500$ s) to show a reduction in COF compared to the other concentrations. The DLC-GNP0.5 COF reduces around 5000 s. The DLC-GNP1 provides a rapid COF reduction followed by a steady-state COF of ~ 0.03 . The DLC-GNP2 contains the highest GNP coverage and follows a similar COF to the DLC-GNP0.5 but increasing rapidly to a COF of ~ 0.07 at $\sim 20,000$

s. The steady state (last 3 h) COF for the samples along with a fully formulated oil (FF) is provided in Fig. 11. The pure DLC provided the highest COF in lubricated conditions in a PAO oil, however the FF use additives such as molybdenum dithiocarbamate (MoDTC) to produce a protective shearing layer to reduce friction and wear, but these can lead to an increase in wear in hydrogenated DLC [38]. The DLC-GNP1 produced the lowest friction with the least deviation.

Fig. 12 shows the wear scars of the DLC-GNP films by SEM along with a representative line. The SEM images of the pure DLC film shows signs of adhesive and abrasive wear, which was also observed in DLC-GNP0.25. The DLC-GNP0.5 shows a smoother wear scar typically observed from a surface polishing wear mechanism, usually obtained through the generation and agglomeration of small third body abrasive particles between the articulating surfaces. These small abrasive particles could be generated by GNP during wear trapping the particles between the surfaces. The DLC-GNP1 displays a clear wear scar but has much less polishing wear observed. The DLC-GNP2 provided more wear than other DLC-GNP samples, and as shown in Fig. 5 large peaks at the GNP islands. Fig. 12(e) presents the wear scar where the GNP islands have been removed during sliding wear. The removal of GNP during wear (and the DLC surrounding the island) would form wear debris in the contact increasing the contact pressure, thus increasing the graphitization, a similar phenomenon is observed by Arslan et al. [66].

The GNP coverage post wear was measured with the results presented in Fig. 13. The coverage for all DLC-GNP samples present a small increase except for the DLC-GNP2 due to the removal of GNP during the wear tests.

The wear rates for the DLC-GNP nanocomposite film along with the CI counter-body are calculated in Fig. 14. It is observed even the lowest GNP/NMP concentration reduces the wear rate of both DLC films and CI counter-body. The wear rate decreases as the GNP/NMP concentration until a concentration of 1 mg/ml is reached. However, concentration above 1 mg/ml increases wear. The increased wear rate could be the result of GNP removed during sliding; this would result in less GNP into the contact area. The wear rates recorded for DLC-GNP nanocomposites is within a factor of the work reported by Wen et al. [67] for GLC films where 4×10^{-18} m³/nm was measured.

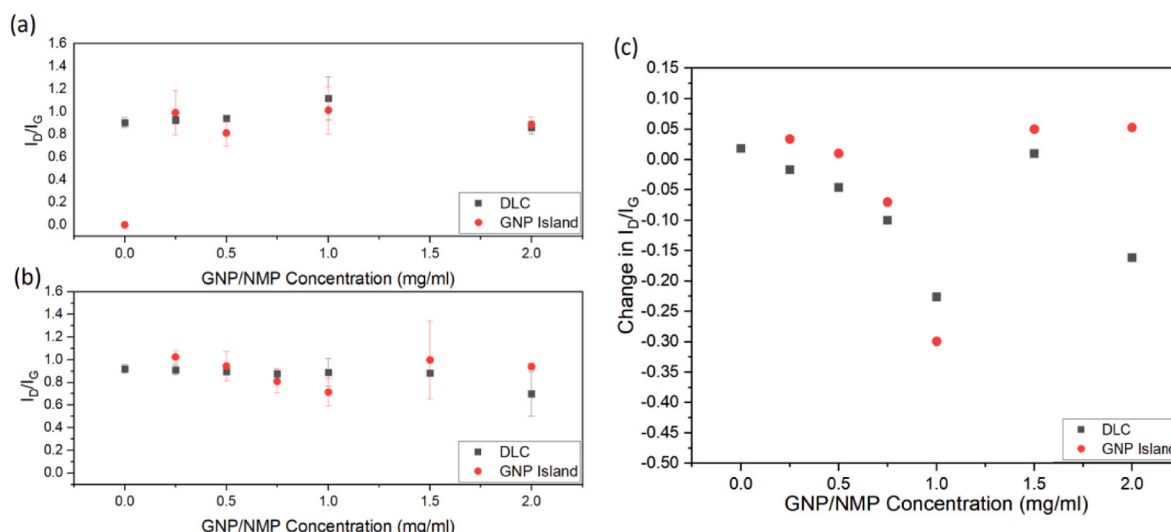


Fig. 16. I_D/I_G Raman spectra for (a) unworn samples and (b) worn samples of various GNP/NMP concentrations. (c) The change in I_D/I_G ratio for the DLC-GNP composites after wear. (A colour version of this figure can be viewed online.)

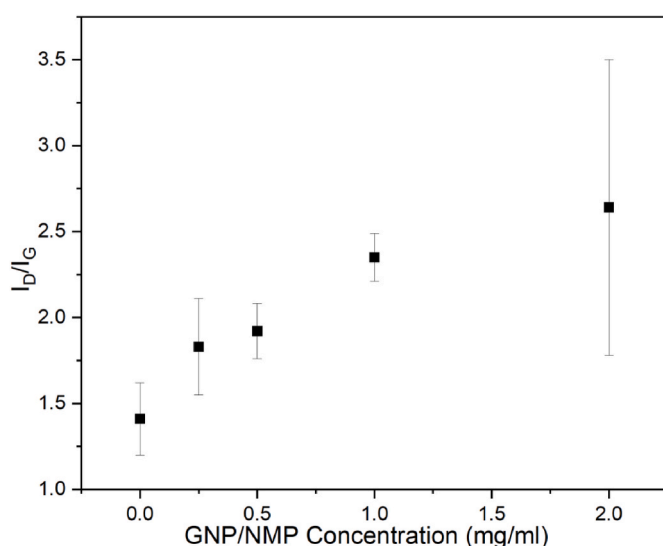


Fig. 17. I_D/I_G ratio for worn CI pins after wear tests against DLC-GNP nanocomposites. (A colour version of this figure can be viewed online.)

3.4. Raman analysis

The Raman spectra of pure DLC, GNP and DLC-GNP (GNP Island) are shown in Fig. 15. For GNP the D ($\sim 1350\text{ cm}^{-1}$) and G ($\sim 1580\text{ cm}^{-1}$) peaks are easy to distinguish, but for pure DLC and DLC-GNP (GNP Island) the spectra needs to be deconvoluted. The penetration depth of

Raman through DLC is reported to be less than $1\text{ }\mu\text{m}$ [68,69] although some reports are as low as 100 nm [70]. The low penetration depth explains the similarity of pure DLC and DLC-GNP spectra for a thickness of $\sim 1.27\text{ }\mu\text{m}$. The collected spectra from the as-deposited DLC-GNP nanocomposites were taken from the GNP islands, and DLC areas using a spot size of 400 nm ensuring the collected area relates only to those discrete areas, and avoiding edge effects.

The I_D/I_G spectra for the as-deposited DLC-GNP nanocomposites is shown in Fig. 16(a). The increases in GNP/NMP concentration does not deviate significantly for DLC areas. The biggest variation for the as-deposited DLC-GNP nanocomposites is from the GNP islands, where again the DLC-GNP1 has the highest value along with the greatest deviation. Fig. 16(b) presents the I_D/I_G ratio for samples after tribological tests were completed. The I_D/I_G ratio for the DLC areas reduce as the GNP/NMP concentration increases with DLC-GNP1 being the lowest. Fig. 16(c) gives the change in I_D/I_G ratio after tribological testing, with the DLC-GNP1 showing a reduction for both DLC and GNP islands areas. The increase in I_D/I_G ratio for the GNP islands post wear could be the result of the DLC above the GNP islands being worn, allowing the counter-body into direct contact with the GNP inducing defects into structure from mechanical wear disrupting the hexagonal lattice which in a perfect crystal is not Raman active, this allows the A1g breathing mode to become active with the spectra and can be observed by a high D peak in the spectra [52,71].

The graphitization process is often credited for the low friction observed for DLC/steel oil lubricated contacts, and often detected by an increases in I_D/I_G ratio [72]. But, no significant increase was observed on the worn surface of the DLC-GNP nanocomposites with the DLC-GNP1 actually showing a reduction [73]. This reduction could be the result of the GNP islands being very close to the surface without

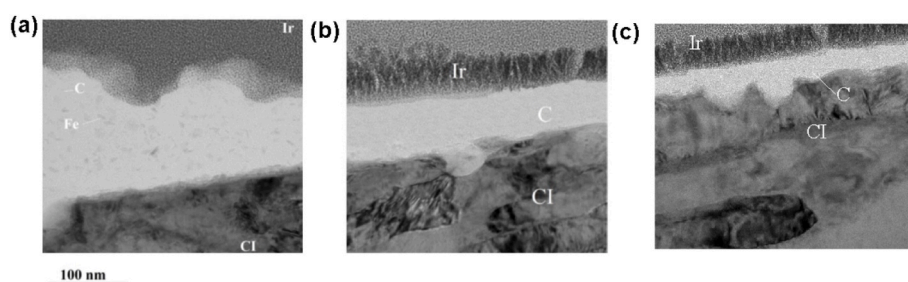


Fig. 18. TEM cross section of (a) Pure DLC, (b) DLC-GNP1, and (c) DLC-GNP2 CI counter after wear. (A colour version of this figure can be viewed online.)

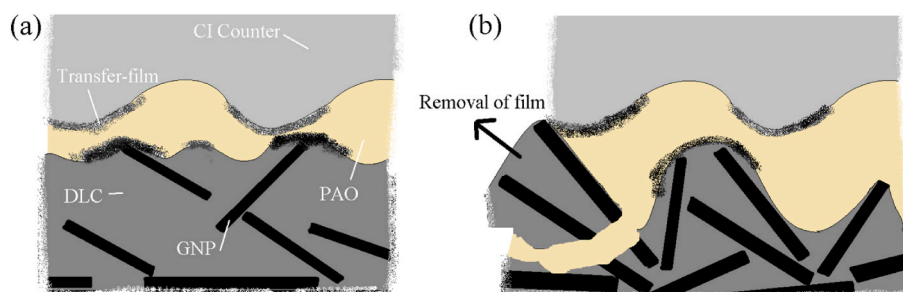


Fig. 19. Mechanism for friction and wear reduction in a DLC-GNP composite with (a) low concentration of GNP, and (b) high concentration of clustered GNPs within the DLC matrix, with removal of high asperity GNP islands. (A colour version of this figure can be viewed online.)

sustaining much damage, or even possibly being sheared without sustaining mechanical abrasive damage. This shearing mechanism could result in transferring carbon to the counter by shearing instead of conventional transformation of $sp^3 \rightarrow sp^2$ carbons creating a more graphitic transfer layer [74]. The I_D/I_G for the DLC-GNP2 is difficult to analyse as there was removal of the GNP islands during the tribological testing, resulting in only the GNP which were not removed being analysed.

Fig. 17 shows the I_D/I_G ratio for the worn pins, which increases with GNP/NMP concentration, demonstrating material transfer from the nanocomposite to the counter-body to form a graphitic transfer film. The lack of formation of a graphitic transfer film on the surface of the DLC-GNP could be the result of any layer being removed during the tribological testing into the oil, but due to greater adhesion between the carbon and cast iron remains on the counter-body [75]. The DLC-GNP2 displaying the highest I_D/I_G ratio which is ~ 2 times that of the pure DLC, but with a high deviation compared to other DLC-GNP samples. The high deviation observed in the DLC-GNP2 is likely due to the removal of the GNP during the wear process, which would greatly reduce the real area of contact for the DLC/CI interface increasing localised contact pressure during sliding and thus facilitating the transformation from $sp^3 \rightarrow sp^2$ bonded carbons forming on the CI pin. Generally, the friction reduces as the I_D/I_G CI transfer layer increases with the exception of DLC-GNP2, where the high surface roughness, combined with peak heights which would lead to greater mechanical locking and higher friction and wear.

TEM cross sections were collected and analysed for pure DLC, DLC-GNP1 and DLC-GNP2 to confirm the presence of a graphitic transfer film Fig. 18. The pure DLC counter presented some Fe crystallites within the graphitic transfer-layer formed. EELS spectra of the counters confirmed sp^2/sp^3 ratio of pure DLC 56.7%, DLC-GNP1 61.0% and DLC-GNP2 65.6%.

4. Friction reduction mechanism

The DLC-GNP composites demonstrate that the addition of GNP into the DLC matrix can improve the friction and wear response. As shown in Fig. 19 as the GNP/NMP concentration increases, the GNP coverage, surface roughness and peak height increase, but the bulk mechanical properties (hardness and elastic modulus) decrease. The decrease in mechanical properties is due to the GNP islands, which with the counter-body creates a reduced real area of contact, increasing contact pressure, graphitization and counter-body transfer film formation, creating a protective low shear graphitic surface [76]. The higher the GNP/NMP concentration becomes, the higher the chances of agglomeration, which introduces sites for crack propagation, and removal of the GNP, along with the DLC surrounding it. The GNP within the DLC matrix form two distinct structures one where the GNP is aligned with the substrate and the other with GNP throughout the DLC, with some penetrating to the surface. It is proposed that the GNP close to the surface is the main source of low shear providing a rich sp^2 carbon layer to the counter-body reducing the friction, faster than observed with pure DLC.

The removal of GNP during the tribological testing of the DLC-GNP2

could be the result of the contact mechanics of very soft GNP islands and a hard DLC film, where combined with high surface roughness, increased the shear and removal of material during wear. This study adds to the work completed Wei et al. [35], where the addition of CNT into DLC had a beneficial impact on the tribological properties, and also increasing the graphitic content (sp^2/sp^3) content.

With the drive towards more efficient coatings graphitic material, in an amorphous carbon matrix could provide benefits of both materials, i. e. an easy shear graphitic layer, with a hard wearing matrix holding the nanomaterial in place at the contact zone. These newly designed nanocomposites could have potential to be used as an alternative to additive packages such as MoDTC which have traditionally shown to increase wear, when used in conjunction with DLC [38].

5. Conclusion

In summary, the addition of GNP into a DLC matrix has shown to have both a friction and wear reducing effect. The effectiveness of the GNP reduces once the GNP/NMP concentration reaches above 1 mg/ml of GNP/NMP, this is due to the GNP clustering at high concentrations and resulting in a high step height, and sites of crack propagation, where they are removed by shearing of the counter-body. The TEM/EELS spectra provide evidence of changes to the sp^2 bonding above the GNP, providing a low shear surface during wear tests until the wear reaches the GNP. The elastic modulus and hardness of the DLC-GNP films is reduced as the coverage of the GNP increases due to different constituents, leading to localised contact pressure differences which may reduce, or increase the real area of contact and provide areas of higher pressures on the DLC matrix facilitating the formation of a highly graphitic transfer film on the counter-body with low shear strength. The formation of the transfer layer on the counter-body seems critical in this system for the low friction and wear, where the I_D/I_G ratio increases as the GNP coverage increases, indicating that although material transfer does occur in pure DLC, the addition of GNP helps increase this process.

Overall, the addition of GNP into a DLC matrix is able to produce a low friction and wear composite that could be suitable in a lubricated environment such as a cam-follower.

CRediT authorship contribution statement

Rob Brittain: Data curation, Writing – original draft, Investigation. **Tomasz Liskiewicz:** Conceptualization, Methodology, Supervision, Writing – review & editing. **Ardian Morina:** Supervision. **Anne Neville:** Supervision. **Liuquan Yang:** Supervision, Writing – review & editing, Project administration, Funding acquisition.

Declaration of competing interest

The authors declare that they have no known competing financial interests or personal relationships that could have appeared to influence the work reported in this paper.

Acknowledgements

This work was funded by Engineering and Physical Sciences Research Council (EPSRC) with the grant titled *EPSRC Centre for Doctoral Training in Integrated Tribology* (EP/L01629X/1). The EPSRC studentship from this grant has the award reference of 1947450. The work was also supported by EPSRC grants titled *Advanced Coatings Platform to Drive New High Value Engineering Processes and Products* (EP/R02524X/1) and *Impact Acceleration Account Phase 3* (EP/R511717/1), respectively.

Appendix A. Supplementary data

Supplementary data to this article can be found online at <https://doi.org/10.1016/j.carbon.2023.01.061>.

References

- [1] A. Grill, Diamond-like carbon: state of the art, *Diam. Relat. Mater.* 8 (1999) 428–434.
- [2] L. Cui, Z. Lu, L. Wang, Probing the low-friction mechanism of diamond-like carbon by varying of sliding velocity and vacuum pressure, *Carbon N Y* 66 (2014) 259–266, <https://doi.org/10.1016/j.carbon.2013.08.065>.
- [3] C. Donnet, A. Erdemir, *Tribology of Diamond-like Carbon Films: Fundamentals and Applications*, Springer US, 2007.
- [4] J. Xu, J. Dai, F. Ren, Y. Wang, P. Wang, S. Xu, et al., Ultrahigh radiation resistance of nanocrystalline diamond films for solid lubrication in harsh radiative environments, *Carbon N Y* 182 (2021) 525–536, <https://doi.org/10.1016/j.carbon.2021.06.056>.
- [5] A. Erdemir, C. Donnet, *Tribology of diamond-like carbon films: recent progress and future prospects*, *J. Phys. D Appl. Phys.* 39 (2006) R311.
- [6] R. Paul, S.N. Das, S. Dalui, R.N. Gayen, R.K. Roy, R. Bhar, et al., Synthesis of DLC films with different sp²/sp³ ratios and their hydrophobic behaviour, *J. Phys. D Appl. Phys.* 41 (2008), 55309.
- [7] A. Tanaka, M. Suzuki, T. Ohana, Friction and wear of various DLC films in water and air environments, *Tribol. Lett.* 17 (2004) 917–924.
- [8] W. Tillmann, E. Vogli, F. Hoffmann, Low-friction diamond-like carbon (DLC)-layers for humid environment, *Thin Solid Films* 516 (2007) 262–266, <https://doi.org/10.1016/j.tsf.2007.06.129>.
- [9] Q. Yu, X. Chen, C. Zhang, J. Luo, Influence factors on mechanisms of superlubricity in DLC films: a review, *Contact Mech. Perspect. Tribol.* 6 (2021).
- [10] M. Kano, Super low friction of DLC applied to engine cam follower lubricated with ester-containing oil, *Tribol. Int.* 39 (2006) 1682–1685.
- [11] M.I.D.B. Bouchet, C. Matta, T. Le-Mogne, J.M. Martin, Q. Zhang, W. Goddard III, et al., Superlubricity mechanism of diamond-like carbon with glycerol. Coupling of experimental and simulation studies, *J. Phys. Conf. Ser.* 89 (2007), 12003. IOP Publishing.
- [12] A. Erdemir, *Diamond-Like Carbon Films and Their Superlubricity*, Superlubricity, Elsevier, 2021, pp. 215–230.
- [13] Y. Liu, A. Erdemir, E.I. Meletis, An investigation of the relationship between graphitization and frictional behavior of DLC coatings, *Surf. Coating. Technol.* 86–87 (1996) 564–568, [https://doi.org/10.1016/S0257-8972\(96\)03057-5](https://doi.org/10.1016/S0257-8972(96)03057-5).
- [14] M. Murashima, S. Oyama, H. Kousaka, T. Tokoroyama, W.-Y. Lee, N. Umehara, New in situ low-friction technology for diamond-like carbon coatings using surface discharge treatment in ambient air, *Tribol. Int.* 165 (2022), 107306, <https://doi.org/10.1016/j.triboint.2021.107306>.
- [15] T.W. Scharf, I.L. Singer, in: C. Donnet, A. Erdemir (Eds.), *Third Bodies and Tribochemistry of DLC Coatings BT - Tribology of Diamond-Like Carbon Films: Fundamentals and Applications*, Springer US, Boston, MA, 2008, pp. 201–236, https://doi.org/10.1007/978-0-387-49891-1_7.
- [16] Y.A.N. Liu, E.I. Meletis, Evidence of graphitization of diamond-like carbon films during sliding wear, *J. Mater. Sci.* 32 (1997) 3491–3495, <https://doi.org/10.1023/A:1018641304944>.
- [17] X. Li, A. Wang, K.-R. Lee, Fundamental understanding on low-friction mechanisms at amorphous carbon interface from reactive molecular dynamics simulation, *Carbon N Y* 170 (2020) 621–629, <https://doi.org/10.1016/j.carbon.2020.08.014>.
- [18] H. Lang, Y. Xu, P. Zhu, Y. Peng, K. Zou, K. Yu, et al., Superior lubrication and electrical stability of graphene as highly effective solid lubricant at sliding electrical contact interface, *Carbon N Y* 183 (2021) 53–61, <https://doi.org/10.1016/j.carbon.2021.07.016>.
- [19] K.-S. Kim, H.-J. Lee, C. Lee, S.-K. Lee, H. Jang, J.-H. Ahn, et al., Chemical vapor deposition-grown graphene: the thinnest solid lubricant, *ACS Nano* 5 (2011) 5107–5114.
- [20] J.H. Warner, F. Schaffel, M. Rummeli, A. Bachmatiuk, *Graphene: Fundamentals and Emergent Applications*, Elsevier Science, 2012.
- [21] R.C. Sinclair, J.L. Suter, P.V. Coveney, Graphene-graphene interactions: friction, superlubricity, and exfoliation, *Adv. Mater.* 30 (2018), 1705791.
- [22] M.M. Van Wijk, M. Dienwiebel, J.W.M. Frenken, A. Fasolino, Superlubric to stick-slip sliding of incommensurate graphene flakes on graphite, *Phys. Rev. B* 88 (2013), 235423.
- [23] M. Tripathi, F. Awaja, R.A. Bizao, S. Signetti, E. Iacob, G. Paolicelli, et al., Friction and adhesion of different structural defects of graphene, *ACS Appl. Mater. Interfaces* 10 (2018) 44614–44623.
- [24] X. Zeng, Y. Peng, H. Lang, A novel approach to decrease friction of graphene, *Carbon N Y* 118 (2017) 233–240, <https://doi.org/10.1016/j.carbon.2017.03.042>.
- [25] D. Berman, S.A. Deshmukh, S.K.R.S. Sankaranarayanan, A. Erdemir, A.V. Sumant, Extraordinary macroscale wear resistance of one atom thick graphene layer, *Adv. Funct. Mater.* 24 (2014) 6640–6646, <https://doi.org/10.1002/adfm.201401755>.
- [26] D. Berman, A. Erdemir, A.V. Sumant, Graphene: a new emerging lubricant, *Mater. Today* 17 (2014) 31–42, <https://doi.org/10.1016/j.mattod.2013.12.003>.
- [27] M.H. Dalal, C.-Y. Lee, G.G. Wallace, Cathodic exfoliation of graphite into graphene nanoplatelets in aqueous solution of alkali metal salts, *J. Mater. Sci.* 56 (2021) 3612–3622, <https://doi.org/10.1007/s10853-020-05468-8>.
- [28] M.F. Arif, H. Alhashmi, K.M. Varadarajan, J.H. Koo, A.J. Hart, S. Kumar, Multifunctional performance of carbon nanotubes and graphene nanoplatelets reinforced PEEK composites enabled via FFF additive manufacturing, *Compos. B Eng.* 184 (2020), 107625, <https://doi.org/10.1016/j.compositesb.2019.107625>.
- [29] Z. Ji, L. Zhang, G. Xie, W. Xu, D. Guo, J. Luo, et al., Mechanical and tribological properties of nanocomposites incorporated with two-dimensional materials, *Friction* 8 (2020) 813–846.
- [30] I. Clavería, S. Gimeno, I. Miguel, G. Mendoza, A. Lostalé, Á. Fernández, et al., Tribological performance of nylon composites with nanoadditives for self-lubrication purposes, *Polymers* 12 (2020) 2253.
- [31] J. Eirina, M. Mariatti, S. Hamdan, Effect of filler loading on the tensile properties of multi-walled carbon nanotube and graphene nanopowder filled epoxy composites, *Procedia Chem.* 19 (2016) 897–905.
- [32] S. Bhowmick, A. Banerji, A.T. Alpas, Friction reduction mechanisms in multilayer graphene sliding against hydrogenated diamond-like carbon, *Carbon N Y* 109 (2016) 795–804.
- [33] Y. Liu, L. Chen, B. Jiang, Y. Liu, B. Zhang, C. Xiao, et al., Origin of low friction in hydrogenated diamond-like carbon films due to graphene nanoscroll formation depending on sliding mode: unidirection and reciprocation, *Carbon N Y* 173 (2021) 696–704.
- [34] D. Berman, S.A. Deshmukh, S.K.R.S. Sankaranarayanan, A. Erdemir, A.V. Sumant, Macroscale superlubricity enabled by graphene nanoscroll formation, *Science* 348 (2015) 1118–1122, 80-.
- [35] C. Wei, C.-I. Wang, F.-C. Tai, K. Ting, R.-C. Chang, The effect of CNT content on the surface and mechanical properties of CNTs doped diamond like carbon films, *Diam. Relat. Mater.* 19 (2010) 562–566, <https://doi.org/10.1016/j.diamond.2010.01.024>.
- [36] H. Kinoshita, I. Ipeei, H. Sakai, N. Ohmae, Synthesis and mechanical properties of carbon nanotube/diamond-like carbon composite films, *Diam. Relat. Mater.* 16 (2007), <https://doi.org/10.1016/j.diamond.2007.08.004>, 1940–4.
- [37] X. Li, W. Dai, Q. Wang, Y. Liang, Z. Wu, Diamond-like/graphite-like carbon composite films deposited by high-power impulse magnetron sputtering, *Diam. Relat. Mater.* 106 (2020), 107818.
- [38] S. Kosarieh, A. Morina, J. Flemming, E. Lainé, A. Neville, Wear mechanisms of hydrogenated DLC in oils containing MoDTC, *Tribol. Lett.* 64 (2016) 4, <https://doi.org/10.1007/s11249-016-0737-0>.
- [39] A. Thornley, Y. Wang, C. Wang, J. Chen, H. Huang, H. Liu, et al., Optimizing the Mo concentration in low viscosity fully formulated oils, *Tribol. Int.* 168 (2022), 107437.
- [40] M. Nakada, Trends in engine technology and tribology, *Tribol. Int.* 27 (1994) 3–8, [https://doi.org/10.1016/0301-679X\(94\)90056-6](https://doi.org/10.1016/0301-679X(94)90056-6).
- [41] D.I. Osman, S.K. Attia, A.R. Taman, Recycling of used engine oil by different solvent, *Egypt. J. Pet.* 27 (2018) 221–225.
- [42] B.D. Beake, T.W. Liskiewicz, V.M. Vishnyakov, M.I. Davies, Development of DLC coating architectures for demanding functional surface applications through nano- and micro-mechanical testing, *Surf. Coating. Technol.* 284 (2015) 334–343, <https://doi.org/10.1016/j.surfcoat.2015.05.050>.
- [43] D. Towery, M.A. Fury, Chapter 6 - Chemical Mechanical Polishing of Organic Polymeric Materials for IC Applications A2 - Nalwa, Hari Singh BT - Handbook of Low and High Dielectric Constant Materials and Their Applications, Academic Press, Burlington, 1999, pp. 241–273, <https://doi.org/10.1016/B978-012513905-2/50008-X>.
- [44] B.J. Hamrock, D. Dowson, Minimum Film Thickness in Elliptical Contacts for Different Regimes of Fluid-Film Lubrication, 1978.
- [45] J. Archard, Contact and rubbing of flat surfaces, *J. Appl. Phys.* 24 (1953) 981–988.
- [46] S. Kosarieh, A. Morina, E. Lainé, J. Flemming, A. Neville, Tribological performance and tribochemical processes in a DLC/steel system when lubricated in a fully formulated oil and base oil, *Surf. Coating. Technol.* 217 (2013) 1–12.
- [47] H. Daniels, A. Brown, A. Scott, T. Nichells, B. Rand, R. Brydson, Experimental and theoretical evidence for the magic angle in transmission electron energy loss spectroscopy, *Ultramicroscopy* 96 (2003) 523–534, [https://doi.org/10.1016/S0304-3991\(03\)00113-X](https://doi.org/10.1016/S0304-3991(03)00113-X).
- [48] Z. Zhang, R. Brydson, Z. Aslam, S. Reddy, A. Brown, A. Westwood, et al., Investigating the structure of non-graphitising carbons using electron energy loss spectroscopy in the transmission electron microscope, *Carbon N Y* 49 (2011) 5049–5063.
- [49] A. Habibi, S.M.M. Khoie, F. Mahboubi, M. Urgan, Raman spectroscopy of thin DLC film deposited by plasma electrolysis process, *Surf. Coating. Technol.* 309 (2017) 945–950.
- [50] A. Eckmann, A. Felten, A. Mishchenko, L. Britnell, R. Krupke, K.S. Novoselov, et al., Probing the nature of defects in graphene by Raman spectroscopy, *Nano Lett.* 12 (2012) 3925–3930.

- [51] E.H. Martins Ferreira, M.V.O. Moutinho, F. Stavale, M.M. Lucchese, R.B. Capaz, C. A. Achete, et al., Evolution of the Raman spectra from single-, few-, and many-layer graphene with increasing disorder, *Phys. Rev. B* 82 (2010), 125429, <https://doi.org/10.1103/PhysRevB.82.125429>.
- [52] A.C. Ferrari, J. Robertson, Interpretation of Raman spectra of disordered and amorphous carbon, *Phys. Rev. B* 61 (2000), 14095.
- [53] G. Gawlik, P. Ciepielewski, J. Jagielski, J. Baranowski, Modification of graphene by ion beam, *Nucl. Instrum. Methods Phys. Res. Sect. B Beam Interact. Mater. Atoms* 406 (2017) 683–688.
- [54] J. Jiang, R.D. Arnell, The effect of substrate surface roughness on the wear of DLC coatings, *Wear* 239 (2000) 1–9, [https://doi.org/10.1016/S0043-1648\(99\)00351-8](https://doi.org/10.1016/S0043-1648(99)00351-8).
- [55] A. Choleridis, S. Sao-Joao, J. Ben-Mohamed, D. Chern, V. Barnier, G. Kermouche, et al., Experimental study of wear-induced delamination for DLC coated automotive components, *Surf. Coating. Technol.* 352 (2018) 549–560, <https://doi.org/10.1016/j.surfcoat.2018.08.048>.
- [56] M. Wissler, Graphite and carbon powders for electrochemical applications, *J. Power Sources* 156 (2006) 142–150, <https://doi.org/10.1016/j.jpowsour.2006.02.064>.
- [57] J. Liu, H.V. Muñoz, K. Nordlund, F. Djurabekova, Structural properties of protective diamond-like-carbon thin films grown on multilayer graphene, *J. Phys. Condens. Matter* 31 (2019), 505703.
- [58] W. Dai, X. Li, L. Wu, Q. Wang, Influences of target power and pulse width on the growth of diamond-like/graphite-like carbon coatings deposited by high power impulse magnetron sputtering, *Diam. Relat. Mater.* 111 (2021), 108232, <https://doi.org/10.1016/j.diamond.2020.108232>.
- [59] B. Hajgató, S. Güryel, Y. Dauphin, J.-M. Blairon, H.E. Miltner, G. Van Lier, et al., Out-of-plane shear and out-of plane Young's modulus of double-layer graphene, *Chem. Phys. Lett.* 564 (2013) 37–40, <https://doi.org/10.1016/j.cplett.2013.02.018>.
- [60] A. Nieto, D. Lahiri, A. Agarwal, Synthesis and properties of bulk graphene nanoplatelets consolidated by spark plasma sintering, *Carbon N Y* 50 (2012) 4068–4077, <https://doi.org/10.1016/j.carbon.2012.04.054>.
- [61] D.-W. Kim, K.-W. Kim, Effects of sliding velocity and normal load on friction and wear characteristics of multi-layered diamond-like carbon (DLC) coating prepared by reactive sputtering, *Wear* 297 (2013) 722–730, <https://doi.org/10.1016/j.wear.2012.10.009>.
- [62] H. Ronkainen, S. Varjus, J. Koskinen, K. Holmberg, Differentiating the tribological performance of hydrogenated and hydrogen-free DLC coatings, *Wear* 249 (2001) 260–266, [https://doi.org/10.1016/S0043-1648\(01\)00558-0](https://doi.org/10.1016/S0043-1648(01)00558-0).
- [63] H. Abdullah Tasdemir, M. Wakayama, T. Tokoroyama, H. Kousaka, N. Umehara, Y. Mabuchi, et al., The effect of oil temperature and additive concentration on the wear of non-hydrogenated DLC coating, *Tribol. Int.* 77 (2014) 65–71, <https://doi.org/10.1016/j.triboint.2014.04.015>.
- [64] E. Rabinowicz, R.I. Tanner, Friction and wear of materials, *J. Appl. Mech.* 33 (1966) 479.
- [65] B. Rübzig, D. Heim, C. Forsich, C. Dipolt, T. Mueller, A. Gebeshuber, et al., Tribological behavior of thick DLC coatings under lubricated conditions, *Surf. Coating. Technol.* 314 (2017) 13–17.
- [66] A. Arslan, H. Masjuki, M. Varman, A. Kalam, R. Mufti, M. Gulzar, et al., Effect of surface texture on the tribological performance of DLC coating, in: *Proc. Malaysian Int. Tribol. Conf.* vol. 246, Malaysian Tribology Society, Malaysia, 2015, 2015.
- [67] S. Wan, J. Pu, D. Li, G. Zhang, B. Zhang, A.K. Tieu, Tribological performance of CrN and CrN/GLC coated components for automotive engine applications, *J. Alloys Compd.* 695 (2017) 433–442, <https://doi.org/10.1016/j.jallcom.2016.11.118>.
- [68] M.A. Tadayoni, N.R. Dando, Normal and surface-enhanced Raman investigations of carbon materials, *Appl. Spectrosc.* 45 (1991) 1613–1616.
- [69] N. Xu, C. Wang, L. Yang, E.K. Barimah, G. Jose, A. Neville, et al., Nano-scale coating wear measurement by introducing Raman-sensing underlayer, *J. Mater. Sci. Technol.* 96 (2022) 285–294, <https://doi.org/10.1016/j.jmst.2021.04.031>.
- [70] M.S. Amer, J. Busbee, S.R. Leclair, J.F. Maguire, J. Johns, A. Voevodin, Non-destructive, in situ measurements of diamond-like-carbon film hardness using Raman and Rayleigh scattering, *J. Raman Spectrosc.* 30 (1999) 947–950.
- [71] D. Sfyris, G.I. Sfyris, C. Galiotis, Stress interpretation of graphene E-2g and A-1g vibrational modes: theoretical analysis, *ArXiv Prepr ArXiv170604465* (2017).
- [72] H.M. Mobarak, E. Niza Mohamad, H.H. Masjuki, M.A. Kalam, K.A.H. Al Mahmud, Friction and wear characteristics of hydrogenated and hydrogen-free DLC coatings when lubricated with biodegradable vegetable oil, *Key Eng. Mater.* 642 (2015) 50–54. *Trans Tech Publ.*
- [73] Y. Guo, P. Guo, L. Sun, X. Li, P. Ke, Q. Li, et al., Tribological properties of Ti-doped diamond-like carbon coatings under dry friction and PAO oil lubrication, *Surf. Interface Anal.* 51 (2019) 361–370.
- [74] A.A. Voevodin, A.W. Phelps, J.S. Zabinski, M.S. Donley, Friction induced phase transformation of pulsed laser deposited diamond-like carbon, *Diam. Relat. Mater.* 5 (1996) 1264–1269, [https://doi.org/10.1016/0925-9635\(96\)00538-9](https://doi.org/10.1016/0925-9635(96)00538-9).
- [75] X. Li, T. Sawaki, H. Kousaka, M. Murashima, N. Umehara, Effect of mating materials on wear properties of amorphous hydrogenated carbon (aC:H) coating and tetrahedral amorphous carbon (ta-C) coating in base oil boundary lubrication condition, *J. Tribol.* 15 (2017) 1–20.
- [76] Q. Ding, L. Wang, Y. Wang, S.C. Wang, L. Hu, Q. Xue, Improved tribological behavior of DLC films under water lubrication by surface texturing, *Tribol. Lett.* 41 (2011) 439–449.